Letter

Optimal Multiplexing of Spatially Encoded Information across Custom-Tailored Configurations of a Metasurface-Tunable Chaotic Cavity

Philipp del Hougne,[1,*] Matthieu Davy,[2] and Ulrich Kuhl[1]

[1] *Institut de Physique de Nice, CNRS UMR 7010, Université Côte d'Azur, 06108 Nice, France*

[2] *Univ Rennes, CNRS, Institut d'Electronique et de Télécommunications de Rennes (IETR) - UMR 6164, F35000 Rennes, France*

(Received 24 January 2020; revised manuscript received 29 February 2020; accepted 20 March 2020; published 24 April 2020)

Tunable disorder-engineered materials offer the opportunity to add functionalities for finely tailored dynamic wave control to applications inevitably or voluntarily based on random materials. Exciting prospects are tailored channel matrices that optimally multiplex information on multiple incoming spatial channels across multiple spatial or configurational channels on the receive side. Here we demonstrate the latter at microwave frequencies based on a chaotic cavity equipped with tunable reflect-array metasurfaces that are configured using a judiciously tailored coding sequence. The results have immediate technological relevance in computational imaging and sensing, since they enable the single-port acquisition of large-aperture spatial information with the lowest possible latency and processing burden. A reduction of the necessary number of measurements by a factor of 2.5 compared with state-of-the-art approaches is found in *in situ* experiments. The proposed concept and platform set the stage for "on-demand" realizations of desired channel-matrix properties and provide fundamental insights into the role of engineered disorder in the interplay of different types of degrees of freedom in mesoscopic physics. The principle is also expected to inspire novel multimode-fiber-based tailored-multiplexing schemes in the optical domain.

DOI: 10.1103/PhysRevApplied.13.041004

The multiplexing of information carried by waves as the waves interact with a complex material (e.g., a multiply scattering layer, a chaotic cavity, a multimode fiber) is a phenomenon underpinning crucial applications such as communication, imaging, and energy transfer [1]. Across disciplines, initial wave-engineering efforts sought to compensate for this information scrambling by shaping the waves incident on the medium. Examples include time-reversal focusing pioneered in acoustics [2], beam forming for wireless communication at radio frequencies [3], and wave-front shaping in the optical domain [4,5]. Later, it became clear that a material's complexity offers wave-manipulation possibilities beyond those available in homogeneous media, leading to applications in which materials causing wave scrambling are introduced on purpose. For instance, subwavelength focusing in optics [6], multispeaker listening in acoustics [7], and computational microwave imaging [8,9] are all enabled by deliberately harnessing a complex medium's property to scramble waves in a seemingly arbitrary manner.

Computational microwave imagers leverage a special case of information scrambling: multiplexing of *spatial* information with *spectral* measurement diversity (see Fig. 1). Waves carrying spatially encoded information about the scene are scrambled by a complex medium and the resulting field is probed at a single position at multiple independent frequencies. This circumvents the need for coherent measurements across large apertures, which are notoriously difficult at radio frequencies. The underlying mechanism is the complete mixing of degrees of freedom (DOF) in complex media irrespective of their nature (e.g., spatial, spectral, polarization), which had previously been evidenced in demonstrations of temporal focusing using spatial DOF and vice versa [10–13]. The frequency diversity of pioneering materials and devices used for multiplexing in the context of computational microwave imaging relied on metamaterial apertures [8,14] or chaotic cavities [9,15,16] with small spectral correlation lengths.

More recently, the use of engineered disordered materials rather than just seemingly arbitrary complex media is emerging in wave engineering. The disorder can be engineered either from scratch [17,18] or through the addition of a tuning mechanism to an initially random medium [19–23]. In the microwave domain, the latter was enabled largely through the emergence of tunable metasurfaces. These artificially engineered ultrathin structures can control electromagnetic wave fronts in a reconfigurable manner and are known as "tunable-impedance surfaces" [24], "programmable-coding metasurfaces" [25], or "spatial microwave modulators" [26]. Combining the tunable-metasurface concept with the complexity of a

*philipp.delhougne@inphyni.cnrs.fr

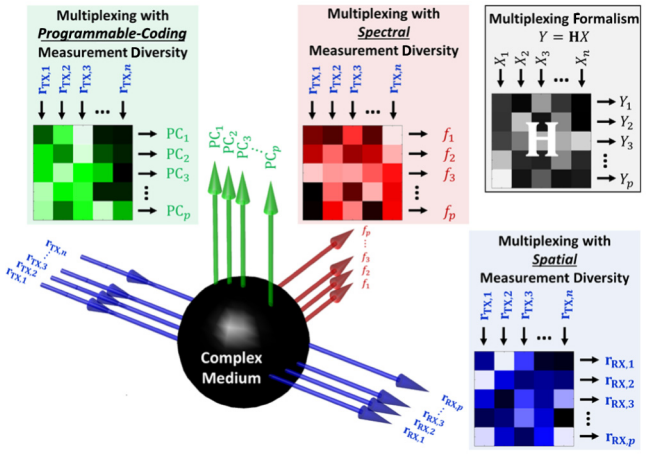

FIG. 1. Principle of information multiplexing with different types of measurement diversity. A complex medium scrambles n pieces of spatially ($\mathbf{r_{TX},}_i$, blue) encoded information. To recover these inputs, the scrambled wave field is probed with p independent measurements, which can be of spatial nature ($\mathbf{r_{RX},}_i$, blue) or spectral nature (f_i, red) or can correspond to different configurations of the complex medium (PC_i, green).

chaotic cavity yields what we refer to as a "programmable-coding metacavity" (PCM) in this work: by partially covering the cavity walls with a reconfigurable reflect-array metasurface as shown in Fig. 2(a), the cavity boundary conditions become programmable, thereby offering large control over the cavity wave field [26–28]. Since a sequence of random PCM coding patterns results in a series of mutually distinct fields inside the PCM, the notion of *programmable-coding* (PC) measurement diversity can be introduced [29–31].

This novel type of DOF enabled a refinement of computational microwave imaging toward single-port

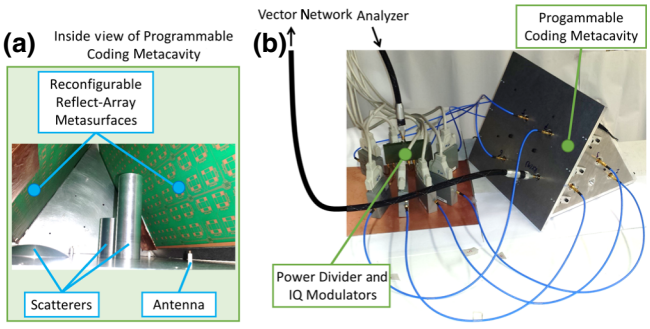

FIG. 2. (a) The programmable coding metacavity (PCM) is an irregular metallic cavity containing scattering objects and two walls are covered by reconfigurable reflect-array metasurfaces. (b) Eight signals, modulated *in situ* by eight in-phase and quadrature (IQ) modulators, excite the cavity via eight antennas. A ninth antenna probes the resulting cavity wave field for different PCM configurations.

single-frequency operation by multiplexing spatial information across a sequence of random PCM coding patterns [29] (see Fig. 1). However, to date the use of PCMs has yet to reap all the benefits offered by the device's programmability. Rather than solely generating a random channel matrix, the PCM can serve as an intelligent platform to custom-tailor the channel-matrix properties through a judiciously chosen coding sequence. Using a tailored coding sequence rather than a random coding sequence does not entail additional hardware cost (both rely on the same PCM) or any speed penalty during operation (both rely on time-sequential measurements).

In this Letter, we report an experimental study of custom-tailoring the space-to-PC channel matrix in a PCM through an optimized coding sequence, considering for concreteness the example of analog multiplexing of spatial information across PCM states. This specific scenario is relevant to computational imaging [29–32] as well as other microwave sensing and metrology applications, such as antenna-array characterization. We show that to match key performance metrics of a channel matrix constructed from a tailored PCM coding sequence, one would have to use a significantly longer random PCM coding sequence, entailing longer acquisition times, greater power consumption, and a larger processing burden. The underlying framework, however, is more general and can be applied to a number of other desirable channel-matrix properties in other contexts [33] that can impact future wave-engineering efforts.

To formalize the concept, we turn to the usual matrix formalism $Y = \mathbf{H}X + N$, where the channel matrix $\mathbf{H}$ links the n incoming spatially encoded pieces of information entering the PCM, X, to the p outgoing measurements with PC diversity through which information is extracted, Y. N denotes the measurement noise vector. The outgoing PC-diverse measurements are taken in a time-sequential manner: each measurement corresponds to a different PCM configuration from the p-element coding sequence; thus, each row of $\mathbf{H}$ is part of a different system's scattering matrix $\mathbf{S}$. This observation differentiates space-to-PC multiplexing from space-to-space multiplexing (encountered, for instance, in wireless communication), where the entire channel matrix is part of a single system's scattering matrix. The profound implications of this difference for the control over $\mathbf{H}$ that can be achieved by judiciously tuning the system's randomness [22] will become clear later.

In analog multiplexing, the overarching goal is to minimize the error of the reconstruction of the incoming spatial information. For the sake of generality, we do not assume any *a priori* knowledge of X or the sensing task motivating us to recover X in the following [34,35]; moreover, we take $\mathbf{H}$ to not be underdetermined (i.e., $p \geq n$). Then, the lowest achievable normalized mean squared error (NMSE) χ of a reconstruction via Tikhonov regularization [36] can be shown [37] to be directly related to the singular-value

(SV) spectrum of the channel matrix:

$$\chi = \frac{1}{n}\sum_{i=1}^{n}\frac{1}{1+\sigma_i^2\rho}, \tag{1}$$

where σ_i is the ith SV of $\mathbf{H}$, $\rho = \|X\|^2/n\zeta^2$ is the signal-to-noise ratio (SNR), and $\zeta = \|N\|/\sqrt{p}$. The reconstruction is thus mainly corrupted by the smallest SVs, which are strongly affected by noise. Ideally, the SV spectrum would therefore be as flat as possible with SV magnitudes as large as possible. Since most practical systems yield a downward-sloping SV spectrum, a conventional method to strengthen the weakest SVs relies on resorting to an overdetermined system ($p > n$) because the smallest normalized SV scales with $\gamma = p/n$ as $\sigma_{\min}/\sqrt{(1/n)\sum_{i=1}^{n}\sigma_i^2} = 1 - \sqrt{1/\gamma}$ [38]. However, this strategy entails costs associated with more measurements. Moreover, the parameter p does not offer flexible and precise control over the SV spectrum. In contrast, with a judiciously chosen PCM coding sequence, the channel-matrix properties can be tailored almost at wish and without using more measurements.

Without knowledge of the SNR and the exact bounds on realizable SV distributions in a given PCM, an optimal accessible SV spectrum cannot be derived analytically from Eq. (1). We hypothesize that at moderate SNRs, maximizing the flatness of the SV spectrum will yield significant improvements of the reconstruction quality by lifting the smallest SVs above the noise level without significantly deteriorating the strongest SVs. Our focus on moderate SNRs is justified since at very high SNRs the smallest SVs are not significantly affected by noise anyway, while at very low SNRs even the strongest SVs are substantially perturbed by noise. To quantify the flatness, we compute the "effective rank" [39] of the channel matrix: $R_{\text{eff}} = \exp\left(-\sum_{i=1}^{n}\tilde{\sigma}_i \ln\tilde{\sigma}_i\right)$, where $\tilde{\sigma}_i = \sigma_i/\sum_{i=1}^{n}\sigma_i$. This metric, essentially the entropy of the SVs, should not be confused with the matrix rank: only a perfectly flat SV spectrum corresponds to $R_{\text{eff}} = n$. R_{eff} is a noninteger quantity suitable for optimization.

Our experimental setup, depicted in Fig. 2 and detailed in Ref. [37], consists of a metallic cavity that contains scattering objects and two of its walls are covered with reconfigurable reflect-array metasurfaces. Here, $n = 8$ monopole antennas inject signals that are individually modulated *in situ* in phase and amplitude into the PCM, while a ninth antenna probes the scrambled wave field. Given the lack of a forward model linking the coding sequence to the resulting channel matrix, we opt for an experimental iterative optimization of the coding sequence as detailed in Ref. [37].

The average downward-sloping SV spectrum of a space-to-PC channel matrix based on a random coding sequence is shown in Fig. 3(a). In an ideal PCM, a perfectly stirred open chaotic system with considerable loss, one would expect to obtain entries of $\mathbf{H}$ distributed as independent zero-mean Gaussian random variables (Rayleigh model) [40,41]. For finite n, such a random matrix has nonvanishing correlations between its rows. Hence, measurements with a random coding sequence inevitably contain some redundant information that does not help to recover X, and consequently the effective rank of such a matrix is never full. We show in Ref. [37] that $\langle R_{\text{eff}}\rangle = 0.8n$ for a random $n \times n$ matrix. Although the distribution of the corresponding eigenvalues of $\mathbf{H}$ in the inset appears to be roughly uniform upon visual inspection, the average effective rank $R_{\text{eff}} = 5.7 \pm 0.3$ is clearly below the value of 6.5 ± 0.2 expected for a random matrix. We attribute this to the persistence of an unstirred field component in the PCM yielding even more correlations between different rows of $\mathbf{H}$ (see Ref. [37]), adding more redundancy and ultimately resulting in an even lower effective rank. As a consequence, the strongest SV is detached from the others (see also the SV distribution in Fig. S5

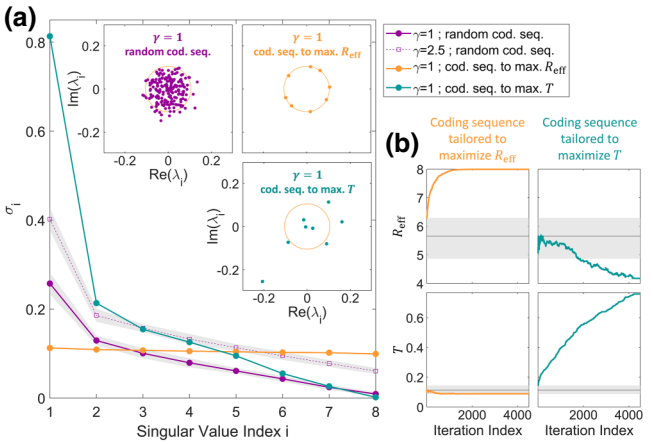

FIG. 3. Dynamics and outcome of tailoring the channel matrix. (a) SV spectra for random channel matrices with $\gamma = 1$ and $\gamma = 2.5$ (averaged over 25 realizations), as well as for a channel matrix with $\gamma = 1$ tailored to maximize R_{eff} or T, respectively. The shaded areas indicate the standard deviations for the cases with random coding sequences. The insets indicate the distribution of the eigenvalues λ_i of $\mathbf{H}$ in the complex plane for 25 random channel matrices with $\gamma = 1$ (top left), for the channel matrix tailored to maximize R_{eff} (top right), and for the channel matrix tailored to maximize T (bottom). For reference, an orange circle is indicated, whose radius is the average magnitude of the eigenvalues for the channel matrix tailored to maximize R_{eff}. (b) Evolution of R_{eff} (top row) and T (bottom row) over the course of the iterative optimization of the coding sequence to maximize R_{eff} (left column) or T (right column). The shaded area and the continuous black line indicate the standard deviation and average, respectively, of the values of R_{eff} and T obtained in 100 random realizations. cod. seq., coding sequence; max., maximize.

[37]). Upon increasing $\gamma = p/n$ from unity to 2.5, the SV spectrum is shifted upward but retains its downward-sloping character. Increasing γ raises the effective rank to 6.6 ± 0.2 and raises the "transmittance," defined as $T = \sum_{i=1}^{n}\sum_{j=1}^{p}|H_{i,j}|^2 = \sum_{i=1}^{n}\sigma_i^2$, from 0.11 ± 0.01 to 0.28 ± 0.03.

Example dynamics of the iterative tailoring of the coding sequence to maximize the effective rank can be seen in Fig. 3(b) to converge to the optimum of $R_{\text{eff}} = n = 8$ after roughly 1200 iterations. Very similar results are obtained in multiple repeats. We observe in Fig. 3(b) that T decreases slightly as we maximize R_{eff}, however not below the minimum value obtained with 100 random coding sequences. Indeed, the final value of $T = 0.09$ is only slightly below the average value for a random coding sequence; only the first two SVs are weaker than their random counterparts, whereas the remaining six are significantly enhanced. The final SV spectrum is flat, and the corresponding complex eigenvalues of $\mathbf{H}$ are equidistant from the origin of the complex plane. Our tailored coding sequence ensures true orthogonality: measurements do not overlap at all such that no redundant information is acquired and we can hope to achieve a given reconstruction quality using fewer measurements.

To put the change in T into perspective, as well as to demonstrate the generality of our approach, we also tailor a coding sequence to maximize T instead of R_{eff}. After 4500 iterations the optimization does not appear to have converged yet but has already reached $T = 0.76$. This huge increase is largely driven by a substantial enhancement of the strongest SV—at the expense of the weaker SVs, which are the most vulnerable to measurement noise. Correspondingly, the anticorrelation between T and R_{eff} is even more striking here: the effective rank drops to 4.2. If we assume that distinct PCM configurations cannot yield exactly the same $T_j = \sum_{i=1}^{n}|H_{i,j}|^2$, it is clear that all p entries of the optimal coding sequence to maximize T would be identical to the coding pattern that yields the largest value of T_j; this observation implies that the global optimum to maximize T inherently corresponds to $R_{\text{eff}} = 1$. This argument highlights a unique feature of a tailored space-to-PC channel matrix, clearly distinguishing it from a space-to-space channel matrix in a programmable environment [22]. In the context of analog multiplexing, the SV spectrum for the coding sequence tailored to maximize T can be expected to yield worse results than a random coding sequence, since its smallest SV is even lower.

We now turn to the improvements in reconstruction quality enabled by tailoring the channel matrix to maximize R_{eff}. We inject *in situ* different input vectors X into the PCM and reconstruct X using Tikhonov regularization based on the measurements Y for a random or tailored coding sequence [37]. Figures 4(a) and 4(d) present typical reconstructions for two inputs at the highest achievable

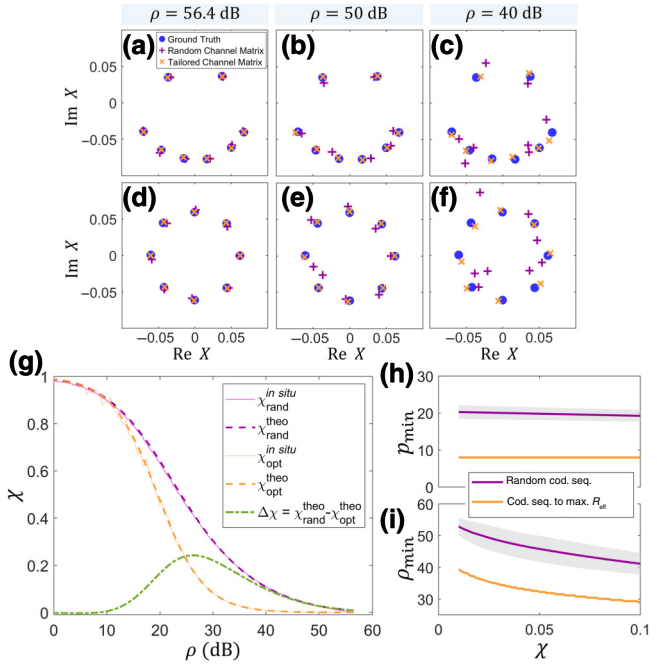

FIG. 4. Reconstruction quality with a random (purple) versus a tailored (orange) channel matrix. (a)–(f) Sample reconstructions of two injected signals (smiley, circle) at three distinct SNRs: 56.4 dB (left), 50.0 dB (middle), and 40.0 dB (right). $\rho = 56.4$ dB is the highest realizable SNR in our experiment. The displayed realizations are chosen such that their reconstruction error is closest to the average reconstruction error. (g) Dependence of the average NMSE, χ, on the SNR, ρ. The corresponding curves for a reconstruction based on *in situ* measurements (continuous lines) are contrasted with the curves dictated by the theory from Eq. (1) (dashed lines). The difference between the two curves for random versus tailored coding sequences is plotted in green. (h) Minimum number of measurements p_{min} necessary to guarantee a given reconstruction quality χ at the SNR at which $p = n$ guarantees this reconstruction quality using the tailored coding sequence. The shaded area indicates the standard deviation when random coding sequences are used. (i) Lowest necessary SNR ρ_{min} that guarantees a given reconstruction quality χ for a system with $\gamma = 1$ for the case of using a random coding sequence or a tailored coding sequence.

experimental SNR ρ of 56.4 dB. We then add synthetically more noise to the measurements to study the performance at lower SNRs; examples for $\rho = 50$ dB and $\rho = 40$ dB are shown in Figs. 4(b) and 4(e) and in Figs. 4(c) and 4(f), respectively. The relation between the NMSE χ and the SNR ρ, as recovered from the *in situ* measurements, is plotted in Fig. 4(g), in excellent agreement with the theory from Eq. (1). As expected, our tailored channel matrix yields the highest enhancements in reconstruction fidelity at moderate SNRs: $\Delta\chi = 24\%$ is achieved around $\rho = 26$ dB.

Figure 4(h) compares the minimum number of measurements needed to ensure a given reconstruction quality χ at the same SNR. In our experiment, 20 measurements

($\gamma = 2.5$) using a random coding sequence are needed to match the performance of eight measurements with a tailored coding sequence. Alternatively, we can ask what minimum SNR is necessary using a random versus a tailored coding sequence of fixed length to guarantee a given reconstruction quality χ. As evident in Fig. 4(i), to ensure, for example, $\chi \leq 5\%$ in our experiment, using eight measurements from a tailored coding sequence rather than a random coding sequence reduces the minimum necessary SNR from 45.6 to 32.4 dB. The superior characteristics of a tailored coding sequence can thus be leveraged to reduce—without any loss in performance—either the number of measurements or the minimum necessary SNR.

Our discussion also highlights that a mathematically rigorous definition of the number of "degrees of freedom" must go beyond an integer quantity directly related to the size of **H**, and hence physical parameters (n, p). Instead, it should be based on the SV spectrum of **H** using noninteger metrics such as the effective rank or the eigenchannel participation number that account for any intrinsic correlations [42,43]. Then the tailored coding sequence can be interpreted as increasing the number of DOF relative to the number available with a random coding sequence, in our case from 5.7 ± 0.3 to the highest possible value of 8.

To summarize, this Letter demonstrates with *in situ* experiments in the microwave domain that using a tailored PCM coding sequence rather than a random PCM coding sequence significantly enhances the performance of analog space-to-PC information multiplexing—without any additional hardware cost or speed penalty during operation. Truly independent measurements are enabled with such a tailored coding sequence. Future work should systematically explore the range of realizable SV spectra in a given PCM, as well as other channel-matrix properties, using learned [44] forward models of a PCM or models capturing the PCM's statistical behavior based on random-matrix theory [45,46]. We also expect our work to inspire conceptually similar efforts in the optical domain, for instance, based on multimode fibers tuned with piezoelectric or acousto-optical modulators [23,47]. Within the more general perspective of engineered wave chaos, the use of reinforcement learning to adapt the tailored PCM coding sequence on the fly to a dynamically evolving application (multiplexing or other) holds great promise.

ACKNOWLEDGMENTS

The authors are supported by the French Agence Nationale de la Recherche under reference ANR-17-ASTR-0017. The metasurface prototypes were purchased from Greenerwave. The authors acknowledge fruitful discussions with Olivier Legrand, Fabrice Mortessagne, and Dmitry Savin.

The project was initiated, conceptualized, and conducted by P.d.H. The derivation of Eq. (1) was proposed by M.D. U.K. provided the experimental equipment and contributed to the design of the experimental setup and the *in situ* realization. All authors thoroughly discussed the results. The manuscript was written by P.d.H. and reviewed by all authors.

[1] P. Sebbah, *Waves and Imaging through Complex Media* (Springer Science & Business Media, Dordrecht, The Netherlands, 2001).

[2] M. Fink, Time reversed acoustics, Phys. Today **50**, 3, 34 (1997).

[3] E. Telatar, Capacity of multi-antenna Gaussian channels, Eur. Trans. Telecomm. **10**, 585 (1999).

[4] I. M. Vellekoop and A. Mosk, Focusing coherent light through opaque strongly scattering media, Opt. Lett. **32**, 2309 (2007).

[5] S. Rotter and S. Gigan, Light fields in complex media: Mesoscopic scattering meets wave control, Rev. Mod. Phys. **89**, 015005 (2017).

[6] I. M. Vellekoop, A. Lagendijk, and A. Mosk, Exploiting disorder for perfect focusing, Nat. Photonics **4**, 320 (2010).

[7] Y. Xie, T.-H. Tsai, A. Konneker, B.-I. Popa, D. J. Brady, and S. A. Cummer, Single-sensor multispeaker listening with acoustic metamaterials, Proc. Natl. Acad. Sci. USA **112**, 10595 (2015).

[8] J. Hunt, T. Driscoll, A. Mrozack, G. Lipworth, M. Reynolds, D. Brady, and D. R. Smith, Metamaterial apertures for computational imaging, Science **339**, 310 (2013).

[9] T. Fromenteze, O. Yurduseven, M. F. Imani, J. Gollub, C. Decroze, D. Carsenat, and D. R. Smith, Computational imaging using a mode-mixing cavity at microwave frequencies, Appl. Phys. Lett. **106**, 194104 (2015).

[10] F. Lemoult, G. Lerosey, J. de Rosny, and M. Fink, Manipulating Spatiotemporal Degrees of Freedom of Waves in Random Media, Phys. Rev. Lett. **103**, 173902 (2009).

[11] J. Aulbach, B. Gjonaj, P. M. Johnson, A. P. Mosk, and A. Lagendijk, Control of Light Transmission through Opaque Scattering Media in Space and Time, Phys. Rev. Lett. **106**, 103901 (2011).

[12] O. Katz, E. Small, Y. Bromberg, and Y. Silberberg, Focusing and compression of ultrashort pulses through scattering media, Nat. Photonics **5**, 372 (2011).

[13] D. J. McCabe, A. Tajalli, D. R. Austin, P. Bondareff, I. A. Walmsley, S. Gigan, and B. Chatel, Spatio-temporal focusing of an ultrafast pulse through a multiply scattering medium, Nat. Commun. **2**, 1 (2011).

[14] J. Gollub, O. Yurduseven, K. Trofatter, D. Arnitz, M. Imani, T. Sleasman, M. Boyarsky, A. Rose, A. Pedross-Engel, and H. Odabasi *et al.*, Large metasurface aperture for millimeter wave computational imaging at the human-scale, Sci. Rep. **7**, 42650 (2017).

[15] T. Fromenteze, C. Decroze, and D. Carsenat, Waveform coding for passive multiplexing: Application to microwave imaging, IEEE Trans. Antennas Propag. **63**, 593 (2014).

[16] T. Fromenteze, E. L. Kpré, D. Carsenat, C. Decroze, and T. Sakamoto, Single-shot compressive multiple-inputs multiple-outputs radar imaging using a two-port passive device, IEEE Access **4**, 1050 (2016).

[17] L. S. Froufe-Pérez, M. Engel, J. J. Sáenz, and F. Scheffold, Band gap formation and Anderson localization in disordered photonic materials with structural correlations, Proc. Natl. Acad. Sci. USA **114**, 9570 (2017).
[18] M. Jang, Y. Horie, A. Shibukawa, J. Brake, Y. Liu, S. M. Kamali, A. Arbabi, H. Ruan, A. Faraon, and C. Yang, Wavefront shaping with disorder-engineered metasurfaces, Nat. Photonics **12**, 84 (2018).
[19] K. G. Makris, A. Brandstötter, P. Ambichl, Z. H. Musslimani, and S. Rotter, Wave propagation through disordered media without backscattering and intensity variations, Light Sci. Appl. **6**, e17035 (2017).
[20] E. Rivet, A. Brandstötter, K. G. Makris, H. Lissek, S. Rotter, and R. Fleury, Constant-pressure sound waves in non-Hermitian disordered media, Nat. Phys. **14**, 942 (2018).
[21] P. del Hougne and G. Lerosey, Leveraging Chaos for Wave-Based Analog Computation: Demonstration with Indoor Wireless Communication Signals, Phys. Rev. X **8**, 041037 (2018).
[22] P. del Hougne, M. Fink, and G. Lerosey, Optimally diverse communication channels in disordered environments with tuned randomness, Nat. Electron. **2**, 36 (2019).
[23] S. Resisi, Y. Viernik, S. M. Popoff, and Y. Bromberg, Wavefront shaping in multimode fibers by transmission matrix engineering, APL Photonics **5**, 036103 (2020).
[24] D. F. Sievenpiper, J. H. Schaffner, H. J. Song, R. Y. Loo, and G. Tangonan, Two-dimensional beam steering using an electrically tunable impedance surface, IEEE Trans. Antennas Propag. **51**, 2713 (2003).
[25] T. J. Cui, M. Q. Qi, X. Wan, J. Zhao, and Q. Cheng, Coding metamaterials, digital metamaterials and programmable metamaterials, Light Sci. Appl. **3**, e218 (2014).
[26] M. Dupré, P. del Hougne, M. Fink, F. Lemoult, and G. Lerosey, Wave-Field Shaping in Cavities: Waves Trapped in a Box with Controllable Boundaries, Phys. Rev. Lett. **115**, 017701 (2015).
[27] P. del Hougne, F. Lemoult, M. Fink, and G. Lerosey, Spatiotemporal Wave Front Shaping in a Microwave Cavity, Phys. Rev. Lett. **117**, 134302 (2016).
[28] P. del Hougne, M. F. Imani, and D. R. Smith, Reconfigurable reflectionless coupling to a metasurface-tunable chaotic cavity, arXiv:2003.01766 (2020).
[29] T. Sleasman, M. F. Imani, J. N. Gollub, and D. R. Smith, Microwave Imaging Using a Disordered Cavity with a Dynamically Tunable Impedance Surface, Phys. Rev. Appl. **6**, 054019 (2016).
[30] P. del Hougne, M. F. Imani, T. Sleasman, J. N. Gollub, M. Fink, G. Lerosey, and D. R.. Smith, Dynamic metasurface aperture as smart around-the-corner motion detector, Sci. Rep. **8**, 1 (2018).
[31] P. del Hougne, M. F. Imani, M. Fink, D. R. Smith, M. Fink, G. Lerosey, Precise Localization of Multiple Noncooperative Objects in a Disordered Cavity by Wave Front Shaping, Phys. Rev. Lett. **121**, 063901 (2018).
[32] M. F. Imani and D. R. Smith, Temporal microwave ghost imaging using a reconfigurable disordered cavity, Appl. Phys. Lett. **116**, 054102 (2020).
[33] N. Bender, H. Yılmaz, Y. Bromberg, and H. Cao, Creating and controlling complex light, APL Photonics **4**, 110806 (2019).
[34] D. L. Donoho, Compressed sensing, IEEE Trans. Inf. Theory **52**, 1289 (2006).
[35] P. del Hougne, M. F. Imani, A. V. Diebold, R. Horstmeyer, and D. R. Smith, Learned integrated sensing pipeline: Reconfigurable metasurface transceivers as trainable physical layer in an artificial neural network, Adv. Sci. **7**, 1901913 (2020).
[36] A. N. Tikhonov, Solution of incorrectly formulated problems and the regularization method, Soviet Math. Dokl. **4**, 1035 (1963).
[37] See Supplemental Material at http://link.aps.org/supplemental/10.1103/PhysRevApplied.13.041004 for additional details on the experimental methods, the link between reconstruction error and SV distribution, and the effective rank of random matrices, and further analysis of the experimental channel matrices.
[38] S. Popoff, G. Lerosey, M. Fink, A. C. Boccara, and S. Gigan, Image transmission through an opaque material, Nat. Commun. **1**, 81 (2010).
[39] O. Roy and M. Vetterli, in *15th European Signal Processing Conference* (IEEE, Poznan, Poland, 2007), p. 606.
[40] J.-H. Yeh, T. M. Antonsen, E. Ott, and S. M. Anlage, First-principles model of time-dependent variations in transmission through a fluctuating scattering environment, Phys. Rev. E **85**, 015202 (2012).
[41] S. Kumar, A. Nock, H.-J. Sommers, T. Guhr, B. Dietz, M. Miski-Oglu, A. Richter, and F. Schäfer, Distribution of Scattering Matrix Elements in Quantum Chaotic Scattering, Phys. Rev. Lett. **111**, 030403 (2013).
[42] M. Davy, Z. Shi, and A. Z. Genack, Focusing through random media: Eigenchannel participation number and intensity correlation, Phys. Rev. B **85**, 035105 (2012).
[43] G. Gradoni, F. Moglie, and V. M. Primiani, Correlation matrix methods to assess the stirring performance of electromagnetic reverberation chambers, Wave Motion **87**, 213 (2019).
[44] S. Ma, B. Xiao, R. Hong, B. Addissie, Z. Drikas, T. Antonsen, E. Ott, and S. Anlage, Classification and prediction of wave chaotic systems with machine learning techniques, Acta Phys. Pol. A **136**, 757 (2019).
[45] U. Kuhl, O. Legrand, and F. Mortessagne, Microwave experiments using open chaotic cavities in the realm of the effective Hamiltonian formalism, Fortschr. Phys. **61**, 404 (2013).
[46] G. Gradoni, J.-H. Yeh, B. Xiao, T. M. Antonsen, S. M. Anlage, and E. Ott, Predicting the statistics of wave transport through chaotic cavities by the random coupling model: A review and recent progress, Wave Motion **51**, 606 (2014).
[47] M. Bello-Jiménez, E. Hernández-Escobar, A. Camarillo-Avilés, O. Pottiez, A. Díez, and M. V. Andrés, Actively mode-locked all-fiber laser by 5 MHz transmittance modulation of an acousto-optic tunable bandpass filter, Laser Phys. Lett. **15**, 085113 (2018).